Materials Today Communications 54 (2026) 115521

Contents lists available at ScienceDirect

Materials Today Communications

journal homepage: www.elsevier.com/locate/mtcomm

Structural, mechanical, electronic, and optical properties of $SnBr_2$ and SnS_2 as functional ceramic semiconductors for optoelectronic and energy applications

Bachir Gueridi [a], Y. Slimani [b], K. Bouferrache [c,d], M.A. Ghebouli [c,e], Samah Saidi [f], Aseel Smerat [g], Murat Yaylacı [h,i], M. Fatmi [c,*]

[a] Laboratory of Physico-chemistry of High Polymers (LPCHP), Department of Process Engineering, Faculty of Technology, Ferhat Abbas University - Setif-1-, Setif 19000, Algeria
[b] Laboratory of Intelligent System (LSI), Faculty of Technology, University Ferhat Abbas of Setif 1, Setif 19000, Algeria
[c] Research Unit on Emerging Materials (RUEM), University Ferhat Abbas of Setif 1, Setif 19000, Algeria
[d] Department of Physics, Faculty of Sciences, University of M'sila University Pole, Road BourdjBouArreiridj, M'sila 28000, Algeria
[e] Department of Chemistry, Faculty of Sciences, University of M'sila University Pole, Road Bourdj Bou Arreiridj, M'sila 28000, Algeria
[f] Department of Physics, College of Science and Humanities in Al-Kharj, Prince Sattam Bin Abdulaziz University, Al-Kharj 11942, Saudi Arabia
[g] Hourani Center for Applied Scientific Research, Al-Ahliyya Amman University, Amman 19328, Jordan
[h] Department of Civil Engineering, Recep Tayyip Erdogan University, Rize 53100, Türkiye
[i] Turgut Kıran Maritime Faculty, Recep Tayyip Erdogan University, Rize 53900, Türkiye

ARTICLE INFO

Keywords:
$SnBr_2$ and SnS_2 compounds
Wien2k
Density functional theory
Electronic structure
Elastic properties
Optical response

ABSTRACT

This work presents a comprehensive first-principles investigation of the structural, mechanical, electronic, and optical properties of layered $SnBr_2$ and SnS_2 compounds, with particular emphasis on their potential as functional ceramic semiconductors. Calculations were performed within the framework of density functional theory using the full-potential linearized augmented plane wave method as implemented in the Wien2k code. Structural optimization was carried out using the generalized gradient approximation, while the modified Becke–Johnson potential was employed to achieve improved accuracy in describing electronic and optical properties. The results confirm that both compounds crystallize in a stable hexagonal structure belonging to the $P6_3/m$ space group and exhibit direct band-gap semiconducting behavior, with band gap values of 2.88 eV for $SnBr_2$ and 2.39 eV for SnS_2. Elastic properties indicate mechanical stability, with $SnBr_2$ showing a ductile tendency and SnS_2 showing a brittle tendency according to the Pugh criterion SnS_2 shows higher mechanical rigidity and stronger bonding characteristics compared to $SnBr_2$, highlighting its suitability for ceramic-based functional applications. Optical analysis reveals absorption coefficients on the order of 10^5 cm^{-1} in the ultraviolet region, along with high refractive indices, indicating appreciable optical response and electronic polarizability. These properties, combined with their calculated band-gap values, suggest that $SnBr_2$ and SnS_2 are potential candidates for ceramic-based optoelectronic devices, UV/visible photodetectors, optical absorbers, and optical-coating applications. Overall, this study provides fundamental insights into the structure–property relationships of Sn-based layered compounds and highlights their potential as functional ceramic semiconductors for optoelectronic and optical-coating applications. This is supported by the clear effect of anion chemistry on the calculated properties, where SnS_2 shows stronger bonding and higher mechanical rigidity than $SnBr_2$, while both compounds maintain dynamical stability, direct band gaps, and appreciable optical absorption.

1. Introduction

Tin-based crystalline semiconductors have attracted increasing attention as functional materials for optoelectronic, photovoltaic, and ceramic-related applications owing to their structural stability, tunable electronic properties, and optical response [1,2]. In these compounds, the physical response is governed not only by chemical composition but also by crystal symmetry, bonding nature, lattice stiffness, elastic

* Corresponding author.
E-mail address: fatmimessaoud@yahoo.fr (M. Fatmi).

https://doi.org/10.1016/j.mtcomm.2026.115521
Received 9 May 2026; Received in revised form 3 June 2026; Accepted 8 June 2026
Available online 8 June 2026

stability, and defect-sensitive electronic structure. Therefore, understanding the relationship between crystal structure and functional properties is essential for evaluating their suitability for optoelectronic and optical applications [3,4]. Among tin-based compounds, layered materials with the general formula SnX_2, where X represents a chalcogen or a halogen, constitute an important class of crystalline semiconductors. Although these systems contain layered structural units, their technologically relevant behavior is strongly associated with their bulk crystalline arrangement, interatomic bonding, mechanical stability, electronic band structure, and optical response. Accordingly, the present work does not focus on isolated two-dimensional monolayers, but rather on the intrinsic structure–property relationships of crystalline SnS_2 and $SnBr_2$ compounds within a unified first-principles framework [5–7]. Within this class, tin dichalcogenides such as SnS_2 have been extensively investigated owing to their favorable electronic band structure, high chemical stability, and promising photocatalytic performance [8,9]. In contrast, tin bromide-based halides exhibit distinct optoelectronic behavior, including strong optical absorption and suitable band gap values, which make them viable candidates for photovoltaic and photonic applications [10]. Notably, the coexistence of ionic and covalent bonding in these compounds introduces additional degrees of freedom for tailoring their electronic and optical responses. The selection of SnS_2 and $SnBr_2$ in the present work is motivated by their representative roles within the SnX_2 family, where the replacement of the anionic species from a chalcogen (S) to a halogen (Br) is expected to strongly affect the bonding nature, lattice stiffness, electronic band structure, and optical response. SnS_2 is a well-known layered chalcogenide semiconductor with reported stability and optoelectronic relevance, whereas $SnBr_2$ represents the halide counterpart with distinct electronic polarizability and optical absorption characteristics. Therefore, studying these two compounds side by side provides a meaningful platform to clarify how the chemical nature of the anion governs the structure–property relationships in Sn-based crystalline layered semiconductors. This comparison is particularly relevant for identifying composition-dependent advantages for optoelectronic and energy-related applications, including photodetection, photodetection, photovoltaic absorber layers, and optical coating technologies.

Despite the growing body of literature on SnX_2 compounds, a critical gap persists in the lack of systematic and comparative investigations that simultaneously address the structural, elastic, electronic, and optical properties of both chalcogenide and halide systems within a unified theoretical framework. Most prior studies have predominantly focused on isolated materials or specific physical properties, thereby limiting a comprehensive understanding of the underlying structure–property relationships. The novelty of the present work lies in providing a unified and comparative first-principles investigation of SnS_2 and $SnBr_2$ as representative chalcogenide and halide members of the SnX_2 family. Unlike previous studies that mainly addressed individual compounds or limited properties, this study simultaneously examines structural stability, elastic behavior, electronic structure, and optical response within the same computational framework. This approach enables a direct evaluation of how the anion chemistry, S versus Br, governs the structure–property relationships and determines the suitability of these compounds for optoelectronic and energy-related applications. It is worth noting that SnS_2-containing heterostructures have been investigated for optoelectronic and energy-related applications, whereas direct first-principles studies on $SnBr_2$ remain relatively limited [11,12]. Therefore, the present work provides a useful comparative assessment of SnS_2 and $SnBr_2$ within the same computational framework, allowing their structural, mechanical, electronic, and optical properties to be evaluated consistently. This lack of direct comparison hinders the rational identification of material-specific advantages and the optimization of these systems for targeted applications. From this perspective, first-principles calculations based on density functional theory (DFT) provide a widely used approach for elucidating the fundamental properties of materials at the atomic scale. The reliability of this computational strategy is further supported by its successful application to several classes of crystalline materials, including oxide ceramics, halide perovskites, Heusler alloys, and doped semiconductors, where first-principles calculations have provided consistent descriptions of structural stability, electronic behavior, optical response, and energy-related properties [13–15]. In particular, the full-potential linearized augmented plane wave (FP-LAPW) method, as implemented in the Wien2k code, is widely regarded as one of the most accurate techniques for describing electronic structure and optical properties of crystalline solids [16,17]. Furthermore, the use of advanced exchange–correlation functionals, such as the modified Becke–Johnson (mBJ) potential, significantly improves the accuracy of band gap predictions, overcoming the well-known limitations of conventional GGA-based approaches [18–20]. Motivated by these considerations, the present study aims to provide a comprehensive and systematic first-principles investigation of SnS_2 and $SnBr_2$ compounds. Specifically, we analyze their structural stability, elastic behavior, electronic band structures, and optical properties within a consistent computational framework. Particular emphasis is placed on elucidating the fundamental differences between the chalcogenide and halide systems and understanding how their chemical composition influences their physical properties. By establishing clear structure–property correlations and benchmarking our results against available theoretical and experimental data, this work seeks to provide valuable insights that can guide the design and optimization of Sn-based materials for advanced optoelectronic applications. In this context, layered Sn-based compounds can be considered as emerging functional ceramic semiconductors due to their structural stability, tunable electronic properties, and strong light–matter interaction. Such characteristics make them particularly attractive for ceramic-based applications including photocatalysis, optical coatings, and energy conversion devices. Therefore, a systematic investigation of their structure–property relationships is essential to assess their potential for integration into advanced ceramic technologies and multifunctional materials design.

2. Computational methodology

First-principles calculations were performed using the Wien2k software package, which implements the full-potential linearized augmented plane wave (FP-LAPW) approach within the density functional theory (DFT) framework [21]. The choice of Wien2k is motivated by the high accuracy of the FP-LAPW method, which treats the crystal potential without shape approximation and provides a reliable all-electron description of crystalline solids. This is particularly important for the present study because accurate electronic band structures, density of states, and optical properties are essential for evaluating the optoelectronic behavior of SnS_2 and $SnBr_2$. To model the exchange-correlation energy, we applied the generalized gradient approximation (GGA) as parameterized by Perdew, Burke, and Ernzerhof (PBE) [22]. Rigorous convergence testing of all computational parameters was conducted to guarantee robust numerical precision. Muffin-tin sphere radii were specified as 2.5 bohr for Sn and Br, and 2.26 bohr for S. Brillouin-zone sampling was carried out over a 1500 k-point mesh. The self-consistent cycles were constrained to converge within 0.0001 Ry for total energy and 0.001 electrons for charge density. The plane-wave expansion cutoff, governed by the product RMT $\times$ Kmax, was fixed at 9. Because standard GGA systematically underestimates semiconductor band gaps, the modified Becke-Johnson (mBJ-GGA) exchange potential was incorporated to yield a more rigorous and accurate representation of the electronic structure [18]. Elastic responses were assessed by imposing small finite strainson the relaxed lattice and evaluating the corresponding stress tensors. Single-crystal elastic constants were extracted from these fitted stress-strain relationships, from which the macroscopic polycrystalline moduli were subsequently derived via the Voigt-Reuss-Hill averaging approximations [23]. Furthermore, optical characteristics were

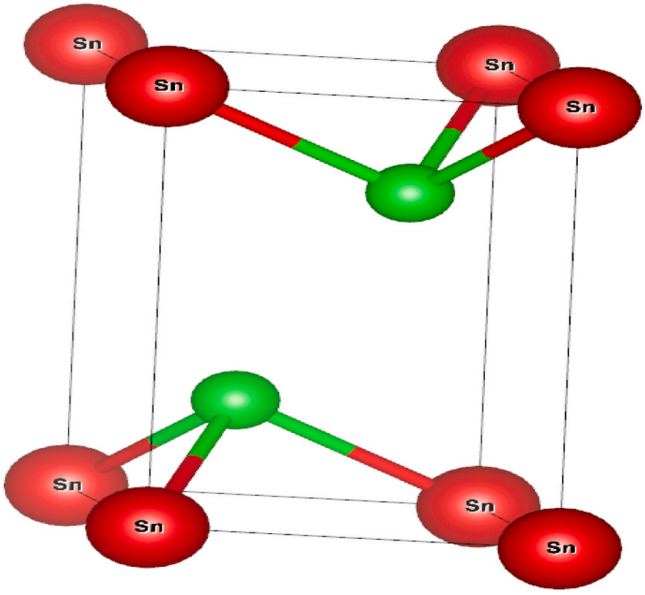

Fig. 1. Crystal structure of SnX_2(X = Br, S) in the hexagonal $P6_3/m$ space group.

Table 1
Calculated lattice parameters a and c, bulk modulus B, pressure derivative of bulk modulus B′, and minimum energy E_o for SnX_2 (X = Br, S) compounds.

Parameters	$SnBr_2$	SnS_2
a(Å)	4.396	3.703 3.651 [30] 3.709 [31]
c(Å)	6.859	5.912 5.88 [30] 5.985 [31]
B(GPa)	27.472	61.569
B′	4.703	4.492
E_0(Ry)	−22784.9773	−13955.13222

simulated across a photon energy spectrum of 0–20 eV using the complex dielectric function $\varepsilon(\omega) = \varepsilon_1(\omega) + i\varepsilon_2(\omega)$. The absorptive imaginary component, $\varepsilon_2(\omega)$, was computed directly from interband electronic transitions, while the dispersive real component, $\varepsilon_1(\omega)$, was deduced using Kramers-Kronig transformations [24]. Finally, to confirm the dynamical stability of the candidate materials, phonon dispersion spectra were mapped by interfacing the Phonopy package with Wien2k, computing interatomic force constants through a finite-displacement supercell methodology [25].

3. Results and discussion

3.1. Structural properties

The compounds $SnBr_2$ and SnS_2 were modeled in a hexagonal crystal structure belonging to the $P6_3/m$ space group (No. 176). Within this configuration, layered arrangements of Sn atoms are octahedrally coordinated by six X atoms (where X = Br, S), and these adjacent layers are held together by weak van der Waals forces (Fig. 1). Table 1 summarizes the outcomes of our structural optimizations. In the case of SnS_2, the theoretically derived lattice constants (a = 3.703 Å, c = 5.912 Å) align closely with both documented empirical data (a = 3.651 Å, c = 5.88 Å) [26] and prior computational assessments (a = 3.709 Å, c = 5.985 Å) [27]. This agreement is further supported by experimental thin-film data reported by Voznyi et al., who found that SnS_2 films exhibit a hexagonal 2H-SnS_2 structure with lattice constants in the ranges a = 3.637–3.647 Å and c = 5.703–5.743 Å, depending on the substrate temperature [28]. The minor positive deviation observed is characteristic of the generalized gradient approximation (GGA) framework and falls within the typical range reported for GGA calculations. Analysis of the bulk moduli, yielded as 27.47 GPa for $SnBr_2$ and 61.57 GPa for SnS_2, indicates higher incompressibility for the sulfide variant. We ascribe this disparity to sulfur's higher electronegativity and more compact ionic radius relative to bromine, which collectively foster stronger chemical bonds in SnS_2. Comparable behaviors have been reported across analogous chalcogenide-halide systems [29]. Furthermore, the energy-volume relationships depicted in Fig. 2 exhibit distinct global minima, thereby supporting the structural stability of these materials. Relative to SnS_2, the energy profile of $SnBr_2$ displays a noticeably wider minimum, a feature that is consistent with its reduced bulk modulus and more compliant bond nature.

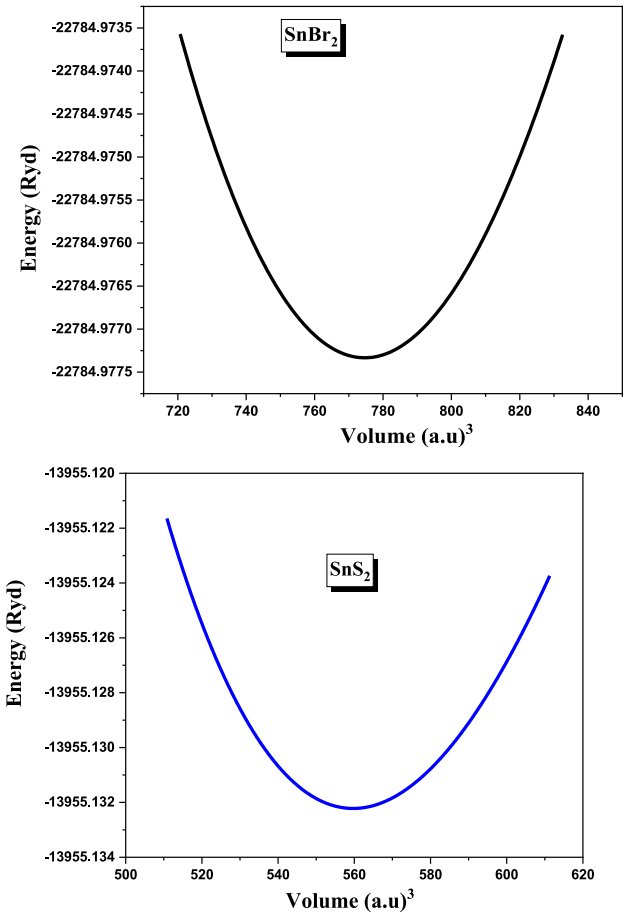

Fig. 2. Energy–volume optimization curves for SnS_2 and $SnBr_2$ using GGA approximation.

The lattice constants computed for SnS_2 align closely with the structural characteristics typical of other layered dichalcogenides. Due to the limited availability of experimental and theoretical mechanical data for the studied $SnBr_2$ and SnS_2 compounds, MoS_2 and WS_2 are introduced here only as representative layered dichalcogenides to provide a reference scale for the mechanical stiffness of SnS_2. This comparison is not intended to imply direct equivalence between these materials, but rather to place the calculated bulk modulus of SnS_2 within the broader family of layered semiconductors. Relative to MoS_2 (a = 3.16 Å, c = 12.3 Å) and WS_2 (a = 3.15 Å, c = 12.4 Å), SnS_2 exhibits an expanded lattice parameter, which is a direct consequence of the Sn^{2+} cation possessing a larger ionic radius than the corresponding transition metals [32,33]. Furthermore, the observed trend in bulk moduli,

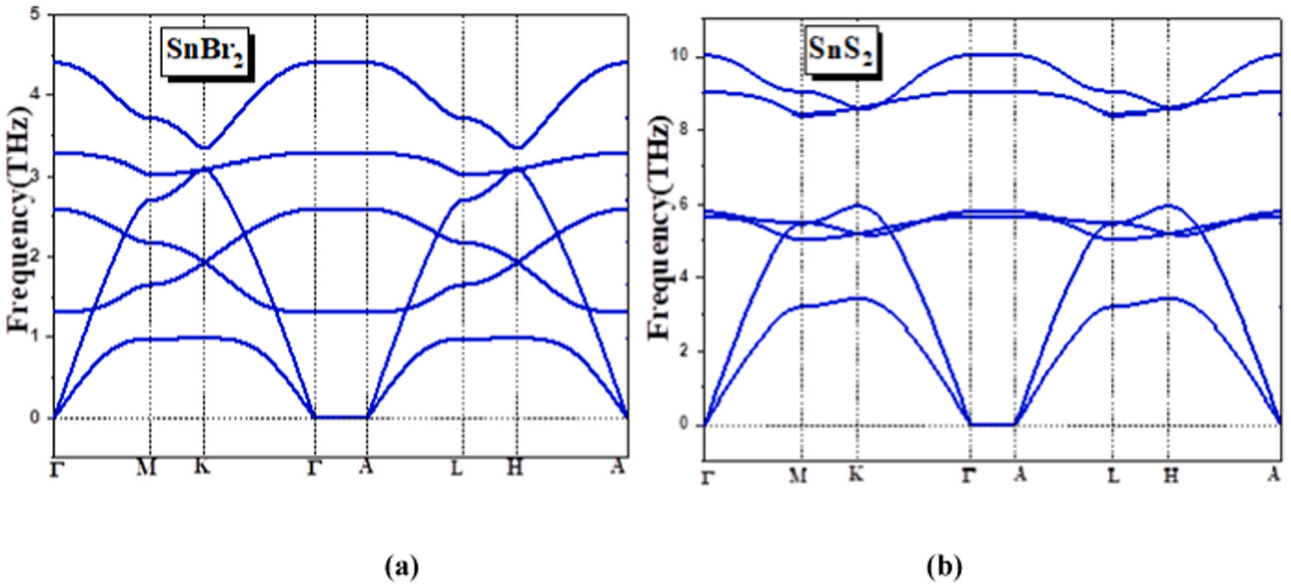

Fig. 3. Phonon dispersions curves for SnS_2 and $SnBr_2$ using GGA approximation.

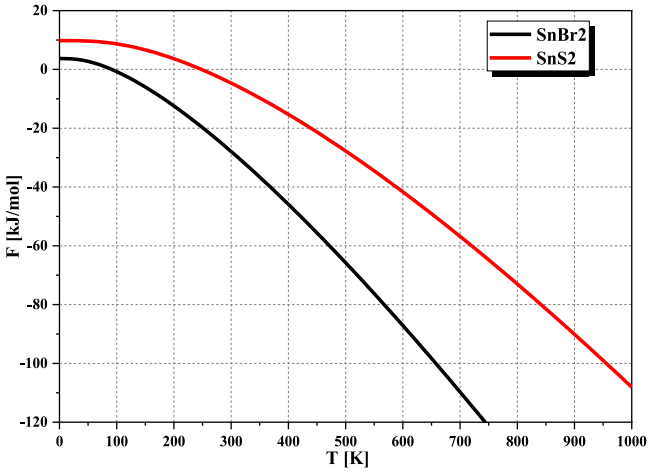

Fig. 4. Helmholtz free energy in the harmonic approximation as function of temperature for SnX_2(X = Br, S) computed by Phononpy Using GGA.

specifically SnS_2 (61.57 GPa) < MoS_2 (238 GPa) < WS_2 (272 GPa), demonstrates that tin dichalcogenides are mechanically more compliant than their transition metal analogs. This reduced stiffness originates from the highly diffuse character of the Sn 5 s orbitals relative to the more localized transition metal d orbitals [34].

3.2. Phonon properties and thermal stability

Fig. 3 depicts the phonon dispersion spectra computed via the generalized gradient approximation (GGA). For both compounds under investigation, the phonon frequencies remain strictly real throughout the entire Brillouin zone, thereby validating their dynamical stability. The complete absence of imaginary modes further substantiates the mechanical stability of the $P6_3/m$ crystal lattice in both $SnBr_2$ and SnS_2. As anticipated, the acoustic branches approach zero frequency at the Γ point and maintain a distinct energetic separation from the optical modes. A comparative analysis reveals that SnS_2 possesses higher overall phonon frequencies compared to $SnBr_2$; this upward shift is a direct consequence of the stronger interatomic bonding and higher elastic moduli inherent to the sulfide material. Finally, the temperature dependence of the Helmholtz free energy, plotted in Fig. 4, exhibits a monotonic reduction as the system temperature is elevated.

3.3. Elastic properties

The calculated single crystal elastic constants (C_{ij}) are listed in Table 2. Both compounds satisfy the mechanical stability criteria for hexagonal crystals:

$$C_{11} > 0,\ C_{33} > 0,\ C_{44} > 0,\ C_{66} > 0 \quad (1)$$

$$(C_{11} + C_{12}) > 0,\ (C_{11} - C_{12}) > 0 \quad (2)$$

$$2(C_{13})^2 < (C_{11} + C_{12})C_{33} \quad (3)$$

Table 2
Single crystal elastic constants, Cij, of SnX_2 (X = Br, S) compounds.

	C_{11}	C_{22}	C_{33}	C_{44}	C_{66}	C_{12}	C_{13}
SnBr2	45.747	45.747	28.831	12.702	13.186	19.376	20.114
SnS2	135.128	135.128	99.060	43.989	43.793	47.542	43.716

Table 3
Calculated bulk modulus B (in GPa), shear modulus G (in GPa), Young's modulus E (in GPa), Poisson's coefficient ν, Pugh's modulus ratio BH/GH and Cauchy pressure, The Kleinman parameter ζ for SnX_2(X = Br, S).

	B_v	B_R	B_H	G_v	G_R	G_H	B/G	E	ν	ζ
$SnBr_2$	26.61	25.24	25.92	11.7	10.9	11.3	2.21	30.7	0.307	0.713
SnS_2	71.029	69.312	70.171	41.977	41.324	41.651	1.68	126.998	0.253	0.606

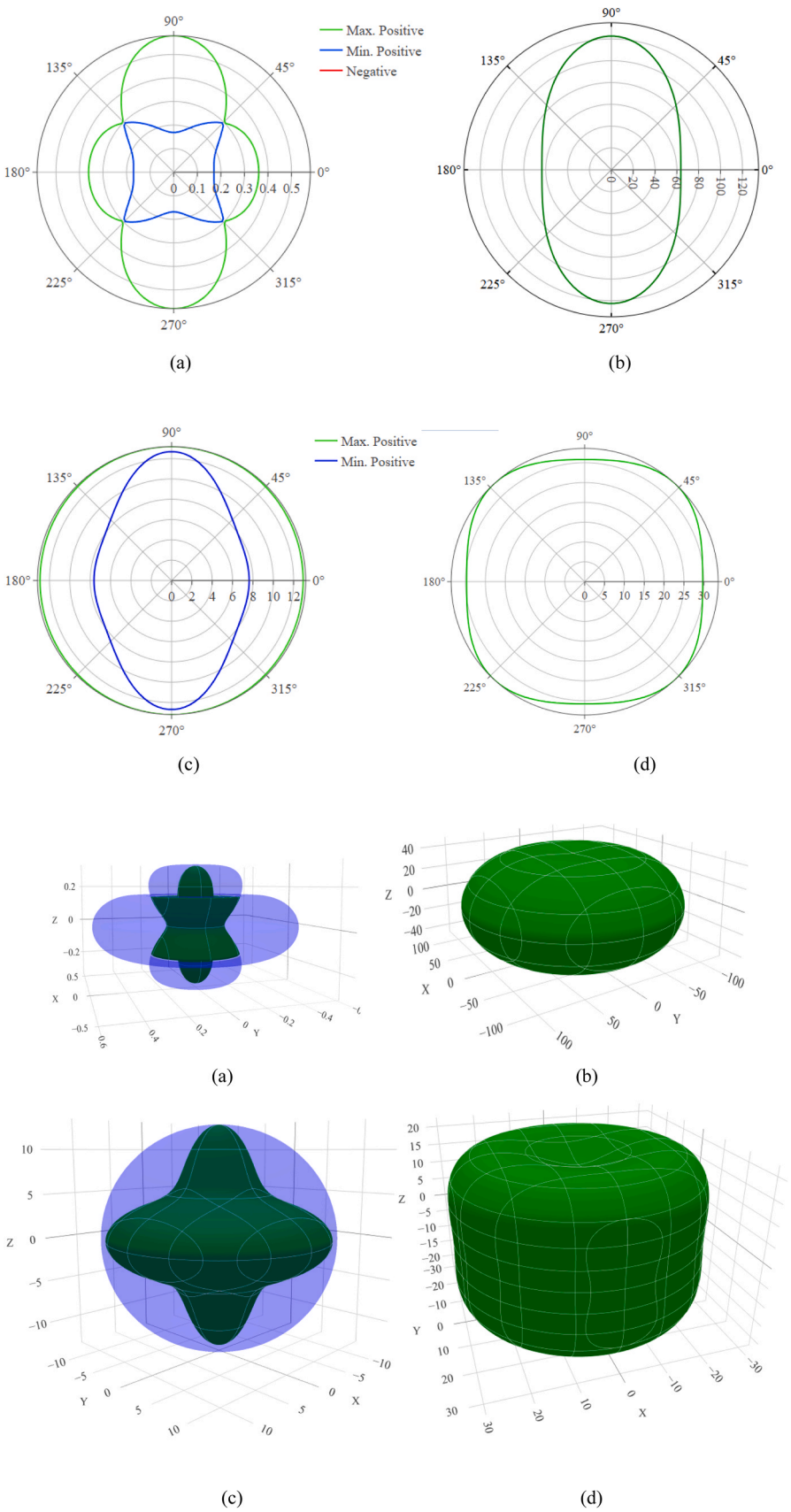

Fig. 5. 2D and 3D Mechanical Properties: (a) Poisson's Ratio, (b) Bulk Modulus, (c) Shear Modulus, and (d) Young's Modulus for $SnBr_2$, respectively.

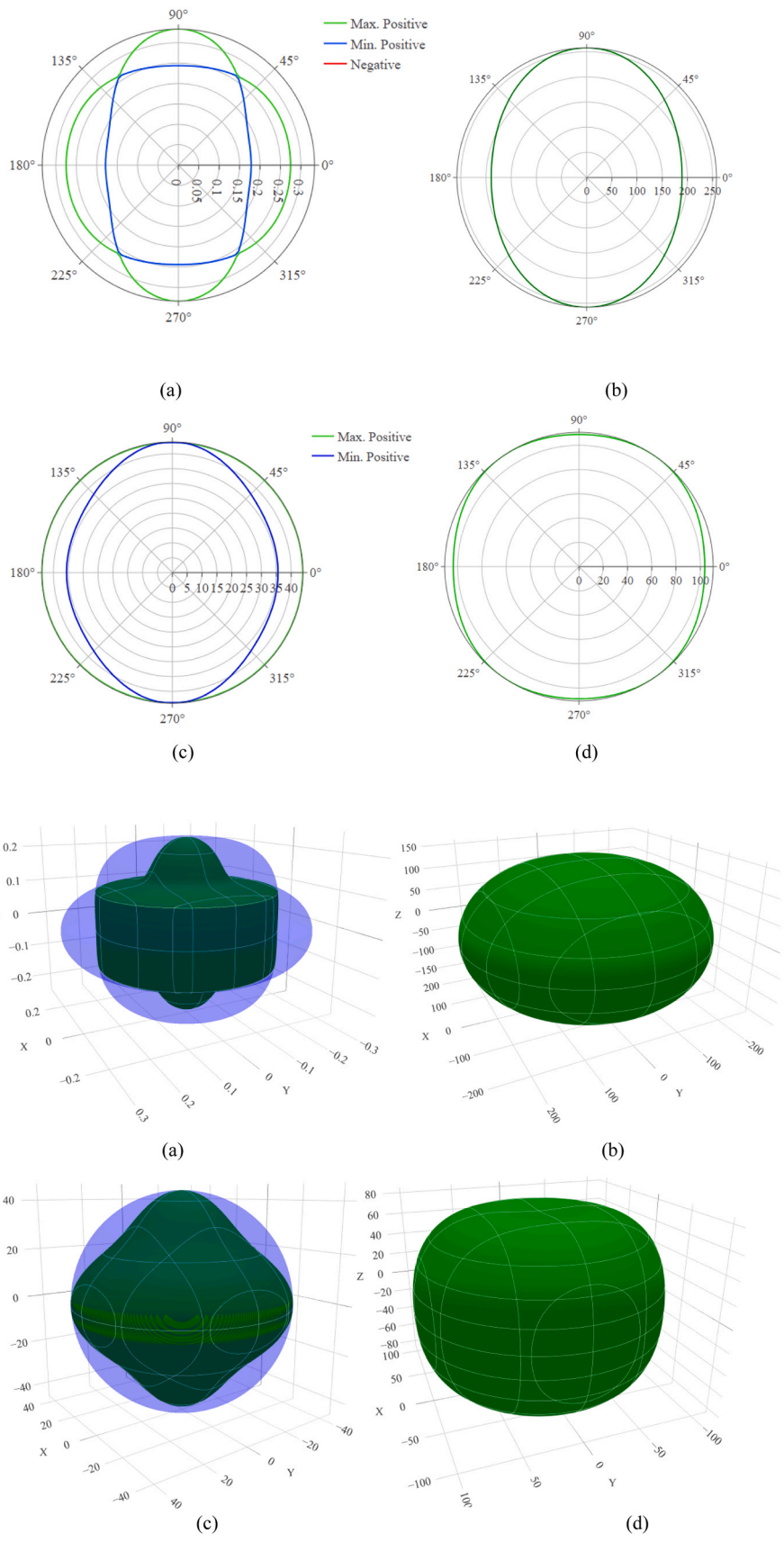

Fig. 6. 2D and 3D Mechanical Properties: (a) Poisson's Ratio, (b) Bulk Modulus, (c) Shear Modulus, and (d) Young's Modulus for SnS_2, respectively.

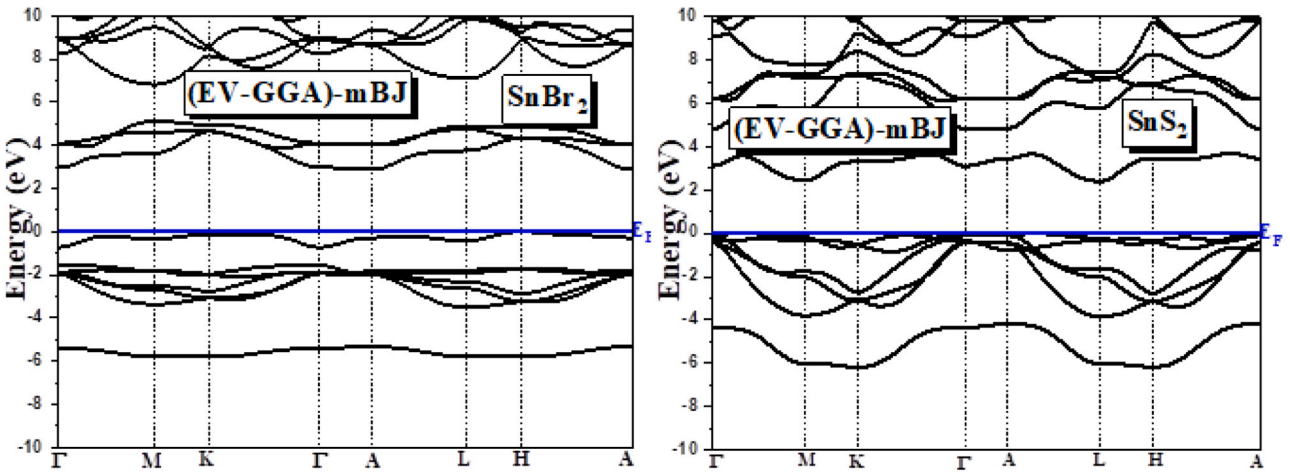

Fig. 7. Electronic Band Structure Calculated Using mBJ-GGA for SnS_2 and $SnBr_2$.

Table 4
Calculated band gap energies of SnX_2 (X = Br, S) compounds using EV-GGA and mBJ-GGA approaches.

	EV-GGA	mBJ
$SnBr_2$	2.34	2.88
SnS_2	1.557	2.39 2.15 [31]

Compared to $SnBr_2$, the elastic constants of SnS_2 are systematically larger, which is indicative of the more robust interatomic bonding characteristic of the chalcogenide. For both compounds, the resistance to c-axis compression quantified by C_{33} (28.83 GPa and 99.06 GPa for SnS_2 and $SnBr_2$, respectively) is notably smaller than the in-plane C_{11} moduli (45.75 GPa and 135.13 GPa, respectively). This disparity highlights the pronounced mechanical anisotropy inherent to these layered structures. Table 3 summarizes the polycrystalline elastic moduli derived via the Voigt-Reuss-Hill approximation. Furthermore, the calculated bulk moduli (25.92 GPa for $SnBr_2$ and 70.17 GPa for SnS_2) agree well with those derived from equation of state fittings, thereby confirming the reliability of our theoretical methodology.

The calculated Pugh's ratios (B/G) are 2.21 and 1.68 for SnS_2 and $SnBr_2$, respectively. Although the standard empirical threshold suggests that B/G > 1.75 typically denotes ductility [35], the present values indicate different mechanical tendencies for the two compounds. $SnBr_2$, with B/G = 2.21, shows a ductile tendency, whereas SnS_2, with B/G = 1.68, is expected to exhibit a brittle tendency according to the Pugh criterion. A similar range of B/G values has also been reported for structurally related layered compounds, such as PbI_2 (B/G = 2.1) and BiI_3 (B/G = 1.9) [36], indicating that layered materials may exhibit different ductile or brittle tendencies depending on their bonding character and elastic response. Mechanical anisotropy is clearly depicted in the 2D projections of the elastic moduli (Fig. 5 and Fig. 6), where pronounced deviations from circular contours signify strong directional dependencies inherent to layered architectures. Notably, SnS_2 exhibits a greater degree of spatial anisotropy compared to $SnBr_2$, a direct consequence of the more robust, directional bonding present in the chalcogenide framework. Additionally, the directional variation of Poisson's ratio, fluctuating between 0.1 and 0.4 based on the specific crystallographic axis, further emphasizes this anisotropic response to mechanical stress. Comprehending such orientation-dependent mechanical traits is fundamental for accurately predicting material performance under varied external loading conditions.

The derived acoustic and thermal parameters further support the difference in mechanical response between the two compounds. SnS_2 exhibits higher transverse, longitudinal, and average elastic wave velocities, with $v_t = 3373.044\ m\ s^{-1}$, $v_l = 5859.865\ m\ s^{-1}$, and $v_a = 3745.704\ m\ s^{-1}$, compared with 1677.366, 3191.791, and 1875.786 m s^{-1} for $SnBr_2$, respectively. This trend is consistent with the higher elastic moduli and stronger bonding network of SnS_2. The Debye

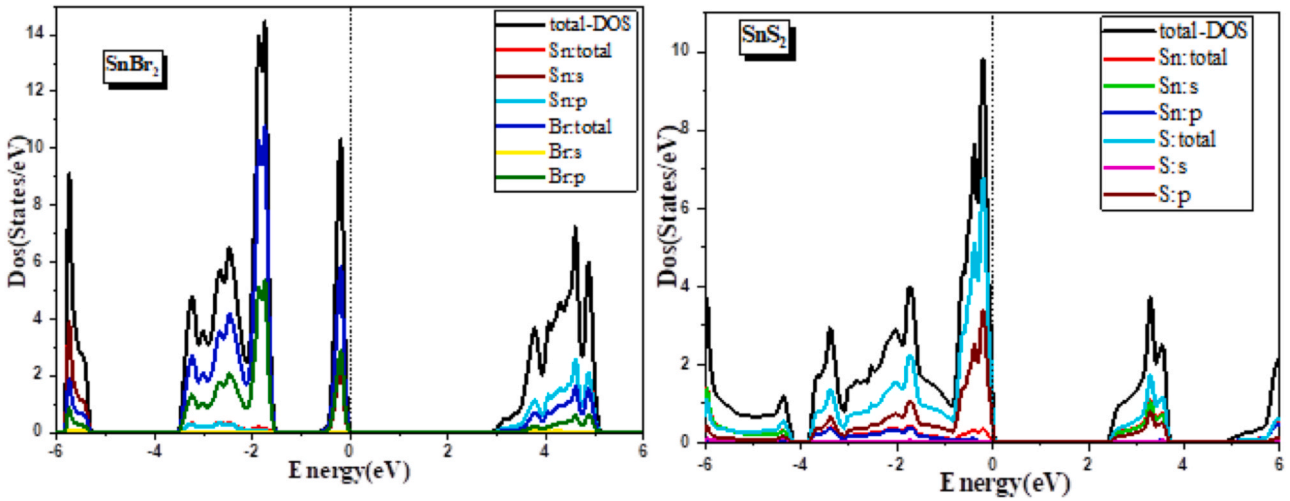

Fig. 8. The density of states of $SnBr_2$ and SnS_2.

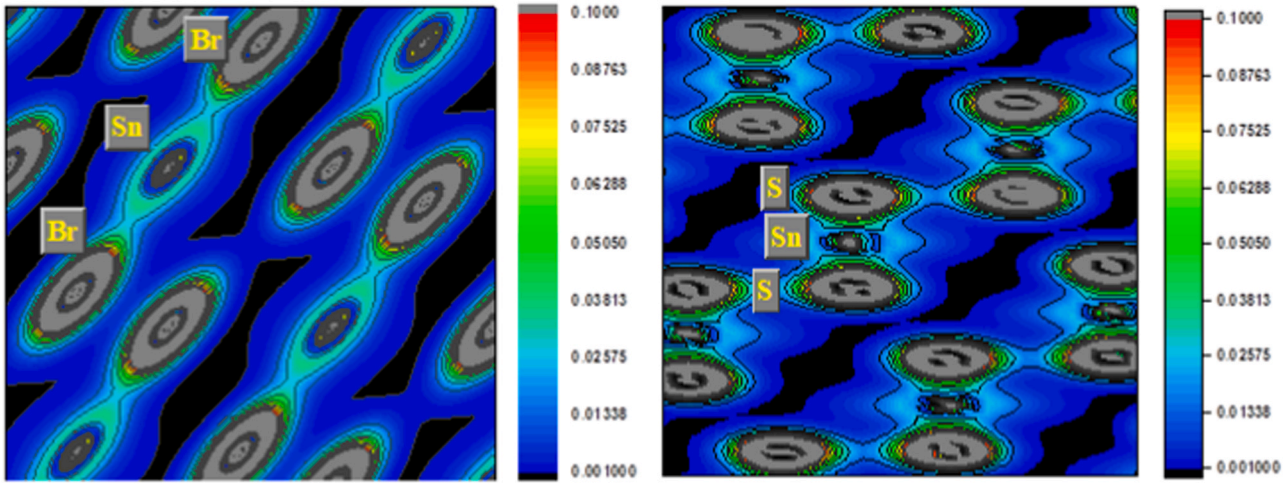

Fig. 9. Charge density distribution of $SnBr_2$ and SnS_2.

temperature also increases from 165.722 K for $SnBr_2$ to 368.810 K for SnS_2, indicating stronger lattice vibrations and relatively higher lattice rigidity in SnS_2. The minimum thermal conductivity was estimated using the Clarke and Cahill models, which provide approximate lower-limit values of the lattice thermal conductivity. In the Clarke model, the minimum thermal conductivity is expressed as $k_{min}{}^{cl} = 0.87\ k^B\ \bar{M}^{-2/3}\ E^{1/2}\ \rho^{1/6}$, where k^B is the Boltzmann constant, $\bar{M}$ is the average atomic mass, E is Young's modulus, and ρ is the density. The Cahill model estimates the minimum thermal conductivity from the acoustic phonon velocities according to $k_{min}{}^{cah} = (k^B / 2.48)\ n^{2/3}\ (v_l + 2v_t)$, where n is the atomic number density, while v_l and v_t are the longitudinal and transverse sound velocities, respectively [37–39]. In addition, SnS_2 has larger minimum thermal conductivity values estimated by the Clarke and Cahill models, 0.701 and 0.919 W m^{-1} K^{-1} , respectively, compared with 0.287 and 0.395 W m^{-1} K^{-1} for $SnBr_2$. These results suggest that SnS_2 possesses a comparatively stiffer and more thermally conductive lattice, whereas $SnBr_2$ is mechanically softer and more compliant.

3.4. Electronic properties

Computations of the electronic band structures for SnS_2 and $SnBr_2$ via the mBJ-GGA approach (Fig. 7) demonstrate direct band gaps. Specifically, both the conduction band minimum (CBM) and the valence band maximum (VBM) are situated at the Γ point, a critical feature that promotes highly efficient radiative recombination suitable for advanced optoelectronic devices. Since conventional GGA is known to systematically underestimate the band gaps of semiconductors and insulators, the modified Becke–Johnson potential within the GGA framework (mBJ-GGA) was employed to obtain a more accurate description of the electronic band structure and optical response [40]. As detailed in Table 4, the predicted band gap energies are 2.88 eV and 2.39 eV for $SnBr_2$ and SnS_2, respectively. For comparison, the calculated mBJ-GGA band gap of SnS_2 is in good agreement with the reported literature value of 2.15 eV [31], confirming the reliability of the present electronic-structure calculations. These estimations present a significant enhancement compared to conventional GGA predictions (2.34 eV and 1.557 eV) and exhibit excellent agreement with prior experimental measurements and theoretical assessments [27,41].

For comparison, Mabiala-Poaty et al. reported a GGA band gap of 1.57 eV for 1T-SnS_2 nanosheets and showed that the valence-band maximum is mainly dominated by S-p states, whereas the conduction-band minimum originates from Sn-s and S-p hybridized states [42]. This is consistent with the orbital contributions observed in the present DOS analysis, confirming the reliability of the calculated electronic structure of SnS_2. The resulting band topologies exhibit prominently flat valence bands, indicative of heavy hole effective masses, alongside highly dispersive conduction bands, which correspond to lighter electron effective masses. Furthermore, profound orbital coupling between Sn 5 s and X p states is observed in the vicinity of the band edges. Evaluating the density of states (DOS) (Fig. 8) reveals that X p orbitals primarily govern the valence band region (spanning −6–0 eV). Conversely, the lower conduction band is predominantly composed of Sn 5 s states. The upper conduction band features contributions from Sn 5p states, whereas the Sn d orbitals manifest as highly localized, narrow bands at lower energy levels between −10 and −12 eV. These electronic characteristics corroborate a mixed ionic-covalent bonding regime. The intrinsic semiconducting nature of these materials originates from substantial electron transfer from the Sn atoms to the X atoms, coupled with robust hybridization of Sn s and X p orbitals adjacent to the Fermi level. Observing the chalcogenide series, the band gap systematically narrows: SnS_2 (2.39 eV) > $SnSe_2$ (1.0 eV) > $SnTe_2$ (metallic). This progression stems from the simultaneous reduction in electronegativity and expansion in atomic radii descending the chalcogen column [43].

Analogously, evaluating isomorphic group IV compounds indicates that GeS_2 possesses a wider band gap (3.65 eV) attributable to more robust Ge-S bonding, whereas relativistic effects inherent to Pb impart metallic characteristics to PbS_2 [44]. Finally, spatial charge density profiles (Fig. 9) verify the accumulation of electrons around the X atoms, underscoring their anionic behavior.

The apparent hole-related behavior can be associated with the flat valence bands and the dominant contribution of anion p states near the valence-band maximum. Since the VBM is mainly governed by Br-p and S-p orbitals, the hole states are expected to be primarily located on the anionic sublattice. However, the present calculations do not claim intrinsic p-type conductivity, since a definitive confirmation would require defect-formation-energy calculations. The Sn-X interactions unequivocally demonstrate a blend of ionic and covalent properties; however, covalent bonding is augmented in SnS_2 owing to the comparatively reduced electronegativity discrepancy between its constituent atoms.

3.5. Optical properties

To obtain more reliable band-gap estimations, the optical characteristics of the SnX_2 compounds were evaluated utilizing the mBJ-GGA functional. The resulting complex dielectric functions and corresponding optical metrics are illustrated in Fig. 10.

Because the investigated compounds crystallize in a hexagonal structure, their optical response is expected to be orientation dependent. The in-plane components, εxx(ω) and εyy(ω), are equivalent by

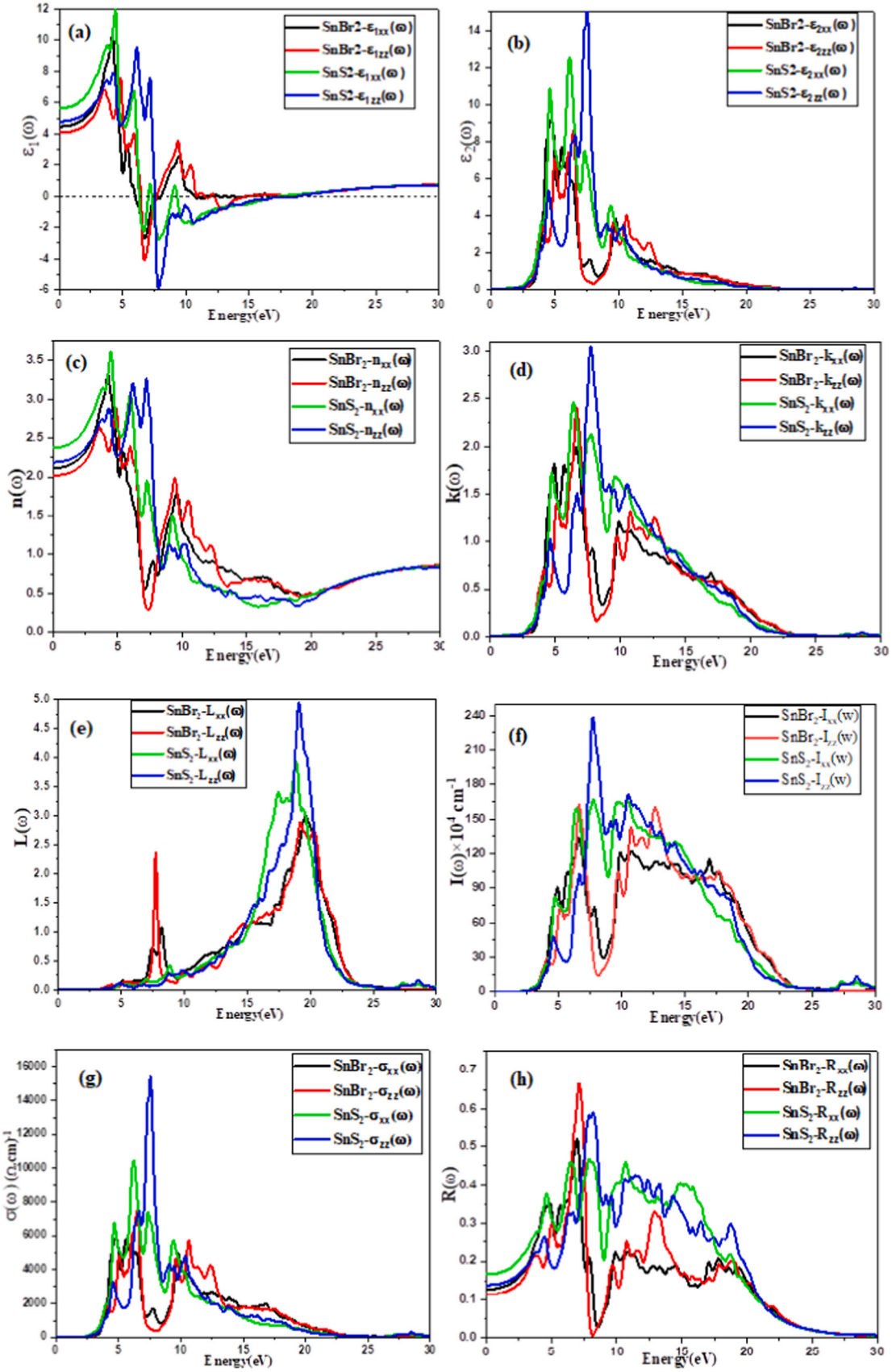

Fig. 10. The real (a) and imaginary (b) components of the dielectric function, the refractive index (c), the extinction coefficient (d), the energy loss (e), and the absorption coefficient (f). The real optical conductivity (g) and reflectivity (h) as functions of photon energy for SnX_2(X = Br, S) calculated using mBJ-GGA.

symmetry, whereas the out-of-plane component, εzz(ω), describes the response along the c-axis. Therefore, the differences between the xx and zz components in Fig. 10 reflect the anisotropic optical behavior of the layered SnX_2 compounds. This anisotropy indicates that light polarized parallel and perpendicular to the c-axis interacts differently with the electronic structure, mainly due to the layered bonding nature and direction-dependent interband transitions. This type of orientation-dependent optical response has also been discussed in recent first-principles studies of anisotropic semiconductors [45]. The real component of the dielectric function, $\varepsilon_1(\omega)$, exhibits elevated static limits specifically, $\varepsilon_1(0) = 8.2$ for $SnBr_2$ and 12.1 for SnS_2. The negative values of $\varepsilon_1(\omega)$ observed at higher photon energies indicate a metallic-like optical response, where the incident electromagnetic wave is strongly screened and cannot propagate efficiently inside the material. This behavior is generally associated with increased reflectivity and plasmonic response near the zero-crossing region of $\varepsilon_1(\omega)$. These figures indicate appreciable electronic polarizability, with the more pronounced magnitude observed in SnS_2 being ascribed to its comparatively narrower band gap coupled with stronger covalent bond strength. Meanwhile, the imaginary part, $\varepsilon_2(\omega)$, displays an absorption threshold that is consistent with the respective band gaps. Prominent peaks emerge between 3 and 4 eV, originating from interband transitions from the valence band (dominated by X-p states) to the conduction band (composed of Sn-s states). In the low-energy regime, the static refractive indices, $n(\omega)$, are approximately 2.9 and 3.5 for $SnBr_2$ and SnS_2, respectively, rendering these materials suitable for applications requiring appreciable optical response and electronic polarizability. Concurrently, the extinction coefficient, $k(\omega)$, mirrors the absorption profile, yielding noticeable magnitudes beyond the band-gap edge and highlighting their potential use in UV/visible photodetection and optical absorber applications.

For both materials, the absorption coefficient, $\alpha(\omega)$, reaches values on the order of 10^5 cm^{-1} in the ultraviolet spectrum. This appreciable UV absorption behavior should be interpreted together with the absorption onset, peak positions, photon-energy range, and calculated band-gap values, rather than from the numerical value alone. This absorption behavior agrees with experimental observations on SnS_2 thin films, where a suitable band-gap range of 2.12–2.44 eV and an optical absorption coefficient higher than 10^4 cm^{-1} were reported, supporting the potential of SnS_2 for optical absorber applications [29]. Owing to its narrower band gap, SnS_2 demonstrates an earlier onset of absorption within the visible light region. Additionally, the optical conductivity, $\sigma(\omega)$, reaches a maximum between 4 and 5 eV, indicating a high probability of interband transitions and efficient generation of charge carriers. Analysis of the energy loss function, $L(\omega)$, identifies distinct plasmonic resonances in the 15–16 eV range. Furthermore, the reflectivity, $R(\omega)$, is sustained above 20% throughout the visible spectrum, a property that may be useful for optical coating and mirror architectures.

When benchmarked against alternative layered semiconductors, the absorption coefficient of SnS_2 on the order of 10^5 cm^{-1} is comparable to that of MoS_2 and higher than that of phosphorene ($\sim 10^4$ cm^{-1}) [46]. Furthermore, the evaluated refractive indices (2.9 for $SnBr_2$ and 3.5 for SnS_2) fall within a favorable range for photonics, situating them competitively relative to values reported for MoS_2 ($n \approx 4.2$) and black phosphorus ($n \approx 3.0$) [47]. Compared with recently reported SnS_2-containing heterostructures, the present results support the potential of SnS_2-containing materials for energy and optoelectronic applications. For instance, SnS_2-containing heterojunctions have been reported as systems with improved photocatalytic behavior when suitable band alignment, enhanced charge separation, and improved optical absorption are achieved [48]. However, such photocatalytic mechanisms are beyond the scope of the present bulk-compound calculations, since no band-edge alignment or surface-reaction analysis was performed in this work. In addition, Sn-based heterostructures such as SnS_2/SnO_2 have shown reported activity in energy-related catalytic processes, further supporting the technological relevance of SnS_2-containing heterostructures [49]. In contrast, to the best of our knowledge, available first-principles data on $SnBr_2$ remain relatively scarce, which highlights the importance of the present comparative study.

4. Conclusions

We report a first-principles investigation of the structural, mechanical, electronic, and optical characteristics of SnX_2 (X = Br, S) employing the Wien2K code. The main findings indicate that both compounds are structurally and dynamically stable, exhibit direct band-gap semiconducting behavior, and show high optical absorption with relatively large refractive indices. The comparative analysis suggests that replacing Br with S strengthens the bonding network and increases the mechanical rigidity of SnS_2, while also modifying the electronic and optical responses. These trends indicate structure–property relationships, where the change from Br to S affects the bonding network, mechanical rigidity, and electronic and optical responses. These theoretical findings provide useful insight into SnX_2 systems and may guide future experimental efforts toward specific optoelectronic applications, such as UV/visible photodetectors, photovoltaic absorbers, and optical coatings. Future work should focus on experimental synthesis, defect-related carrier behavior, strain engineering, and device-level performance evaluation to further validate and optimize these SnX_2 compounds.

CRediT authorship contribution statement

Aseel Smerat: Data curation. **Murat Yaylacı:** Data curation, Conceptualization. **Fatmi M:** Validation, Methodology. **Bachir Gueridi:** Data curation. **MA. Ghebouli:** Investigation, Formal analysis. **Samah Saidi:** Data curation. **Y. Slimani:** Data curation, Conceptualization. **K. Bouferrache:** Investigation, Data curation.

Ethics declaration

Not Applicable.

Funding

None.

Declaration of Competing Interest

The authors declared no potential conflicts of interest with respect to the research, authorship, and/or publication of this article.

Acknowledgments

This study is supported via funding from Prince Sattam bin Abdulaziz University project number (PSAU/2026/R/1447)

Data availability

No data was used for the research described in the article.

References

[1] L.A. Burton, et al., Electronic and optical properties of single crystal SnS_2: an earth-abundant disulfide photocatalyst, J. Mater. Chem. A 4 (2016) 1312–1318, https://doi.org/10.1039/C5TA08214E.
[2] B. Evans, R. Hazelwood, Optical and electrical properties of SnS_2, J. Phys. D Appl. Phys. 2 (1969) 1507–1516, https://doi.org/10.1088/0022-3727/2/11/304.
[3] A. Voznyi, V. Kosyak, A. Opanasyuk, N. Tirkusova, L. Grase, A. Medvids, G. Mezinskis, Structural and electrical properties of SnS_2 thin films, Mater. Chem. Phys. 173 (2016) 52–61.
[4] M.J. Powell, The effect of pressure on the optical-absorption edge in SnS_2 and $SnSe_2$, Il Nuovo Cim. B 38 (1977) 384–392, https://doi.org/10.1016/j.matchemphys.2016.01.036.

[5] P. Eckold, W. Hügel, Robert E. Dinnebier, R. Niewa, Two modifications of tin(II) bromide, Z. Anorg. Allg. Chem. 641 (2015) 1467–1472, https://doi.org/10.1002/zaac.201500108.

[6] M. Kolonits, B. Réffy, G. Jancsó, M. Hargittai, Molecular structure and thermochemistry of tin dibromide monomers and dimers: a computational and electron diffraction study, J. Phys. Chem. A 108 (2004) 6778–6783, https://doi.org/10.1021/jp048667l.

[7] L. Lang, Ji-Hui Yang, Heng-Rui Liu, H.J. Xiang, X.G. Gong, First-principles study on the electronic and optical properties of cubic ABX_3 halide perovskites, Phys. Lett. A 378 (2014) 290–293, https://doi.org/10.1016/j.physleta.2013.11.018.

[8] Lee A. Burton, D. Colombara, Ruben D. Abellon, Ferdinand C. Grozema, Laurence M. Peter, Tom J. Savenije, G. Dennler, A. Walsh, Synthesis, characterization, and electronic structure of single-crystal SnS, Sn_2S_3, and SnS_2, Chem. Mater. 25 (2013) 4908–4916, https://doi.org/10.1021/cm403046m.

[9] A.A. Tedstone, D.J. Lewis, P. O'Brien, Synthesis, properties, and applications of transition metal-doped layered transition metal dichalcogenides, Chem. Mater. 28 (2016) 1965–1974, https://doi.org/10.1021/acs.chemmater.6b00430.

[10] L. Lang, Ji-Hui Yang, Heng-Rui Liu, H.J. Xiang, X.G. Gong, First-principles study on the electronic and optical properties of cubic ABX_3 halide perovskites, Phys. Lett. A 378 (2014) 290–293, https://doi.org/10.1016/j.physleta.2013.11.018.

[11] F.A. Bensaber, B. Amiri, B. Bouabdallah, I. Bouchama, S. Alomairy, M.A. Ghebouli, M. Fatmi, B. Ghebouli, M.J.A. Abualreish, A. Smerat, The Potential of Tm-Doped GaN: a comprehensive study of magnetic, optical, and thermoelectric properties for optoelectronic and energy conversion applications, J. Supercond. Nov. Magn. 39 (2026) 81, https://doi.org/10.1007/s10948-026-07176-x.

[12] K. Bouferrache, M.A. Ghebouli, Samah Saidi, M. Fatmi, M.J.A. Abualreish, A. Smerat, M. Yaylaci, Structural, electronic, mechanical and optical properties of $Pu_{1-x}Th_xO_2$ fluorite ceramics: a first-principles study, Mater. Today Commun. 53 (2026) 115356, https://doi.org/10.1016/j.mtcomm.2026.115356.

[13] K. Bouferrache, M.A. Ghebouli, M. Fatmi, B. Ghebouli, F.K. Alanazi, M.J. A. Abualreish, A. Smerat, M. Yaylaci, First-principles insights into structural, elastic, electronic, optical, and thermoelectric properties of $ZnRh_2O_4$ spinel oxide ceramic, J. Korean Ceram. Soc. (2026), https://doi.org/10.1007/s43207-026-00616-3.

[14] M.A. Ghebouli, K. Bouferrache, B. Ghebouli, M. Fatmi, S. Alomairy, M. Yaylaci, A. Smerat, M.J.A. Abualreish, First-principles calculations to investigate structural, electronic, optical, thermoelectric and NMR properties of K_2PtCl_6 for optoelectronic and energy conversion applications, Mater. & Des. 265 (2026) 115932, https://doi.org/10.1016/j.matdes.2026.115932.

[15] R. Ameur, K. Bouferrache, A. Guibadi, M.A. Ghebouli, B. Ghebouli, M. Fatmi, F. K. Alanazi, Half-metallicity and spin-gapless semiconducting properties in FeCrTiM (M = Al, As, Si) quaternary Heusler alloys for spintronic, thermoelectric and optoelectronic applications, Adv. Compos. Hybrid. Mater. 8 (2025) 366, https://doi.org/10.1007/s42114-025-01466-z.

[16] M.D. Segall, P.J.D. Lindan, M.J. Probert, C.J. Pickard, P.J. Hasnip, S.J. Clark, M. C. Payne, First-principles simulation: Ideas, illustrations and the CASTEP code, J. Phys. Condens. Matter 14 (2002) 2717–2744, https://doi.org/10.1088/0953-8984/14/11/301.

[17] P. Blaha, K. Schwarz, G.K.H. Madsen, D. Kvasnicka, J. Luitz, R. Laskowski, F. Tran, L.D. Marks, WIEN2k: An Augmented Plane Wave plus Local Orbitals Program for Calculating Crystal Properties, Vienna University of Technology, Austria, 2018.

[18] F. Tran, P. Blaha, Accurate band gaps of semiconductors and insulators with a semilocal exchange-correlation potential, Phys. Rev. Lett. 102 (2009) 226401, https://doi.org/10.1103/PhysRevLett.102.226401.

[19] D.J. Singh, Electronic structure calculations with the Tran–Blaha modified Becke–Johnson density functional, Phys. Rev. B 82 (2010) 205102, https://doi.org/10.1103/PhysRevB.82.205102.

[20] J.A. Camargo-Martínez, R. Baquero, Performance of the modified Becke–Johnson potential for semiconductors, Phys. Rev. B 86 (2012) 195106, https://doi.org/10.1103/PhysRevB.86.195106.

[21] D.J. Singh, L. Nordstrom. Planewaves, Pseudopotentials, and the LAPW Method, 2nd ed., Springer, New York, 2006.

[22] J.P. Perdew, K. Burke, M. Ernzerhof, generalized gradient approximation made simple, Phys. Rev. Lett. 77 (1996) 3865–3868, https://doi.org/10.1103/PhysRevLett.77.3865.

[23] R. Hill, The elastic behaviour of a crystalline aggregate, Proc. Phys. Soc. A 65 (1952) 349–354, https://doi.org/10.1088/0370-1298/65/5/307.

[24] F. Wooten, Optical Properties of Solids, Academic Press, New York, 1972.

[25] A. Togo, I. Tanaka, First principles phonon calculations in materials science, Scr. Mater. 108 (2015) 1–5, https://doi.org/10.1016/j.scriptamat.2015.07.021.

[26] L.S. Price, I.P. Parkin, A.M.E. Hardy, R.J.H. Clark, T.G. Hibbert, K.C. Molloy, Atmospheric pressure chemical vapor deposition of tin sulfides (SnS, Sn_2S_3, and SnS_2) on glass, Chem. Mater. 11 (1999) 1792–1799, https://doi.org/10.1021/cm990005z.

[27] Y. Javed, M.A. Rafiq, N. Ahmed, Pressure-induced changes in the electronic structure and enhancement of the thermoelectric performance of SnS_2: a first principles study, RSC Adv. 7 (2017) 38834–38843, https://doi.org/10.1039/C7RA06455A.

[28] A. Voznyi, V. Kosyak, A. Opanasyuk, N. Tirkusova, L. Grase, A. Medvids, G. Mezinskis, Structural and electrical properties of SnS_2 thin films, Mater. Chem. Phys. 173 (2016) 52–61, https://doi.org/10.1016/j.matchemphys.2016.01.036.

[29] A. Shafique, Y.H. Shin, Strain engineering of phonon thermal transport properties in monolayer 2H-$MoTe_2$, Phys. Chem. Chem. Phys. 19 (2017) 32072–32078, https://doi.org/10.1039/C7CP06065C.

[30] L.S. Price, I.P. Parkin, A.M.E. Hardy, R.J.H. Clark, T.G. Hibbert, K.C. Molloy, Atmospheric pressure chemical vapor deposition of tin sulfides (SnS, Sn2S3, and SnS2) on Glass, Chem. Mater. 11 (1999) 1792–1799, https://doi.org/10.1021/cm990005z.

[31] Y. Javed, A. Rafiq M, N. Ahmed, Pressure-induced changes in the electronic structure and enhancement of the thermoelectric performance of SnS2: a first principles study, RSC Adv. 7 (2017) 38834–38843, https://doi.org/10.1039/C7RA06455A.

[32] H. Shi, H. Pan, Y.W. Zhang, B.I. Yakobson, Quasiparticle band structures and optical properties of strained monolayer MoS_2 and WS_2, Phys. Rev. B 87 (2013) 155304 https://doi.org/10.1103/PhysRevB.87.155304.

[33] K.F. Mak, C. Lee, J. Hone, J. Shan, T.F. Heinz, atomically thin MoS_2: a new direct-gap semiconductor, Phys. Rev. Lett. 105 (2010) 136805, https://doi.org/10.1103/PhysRevLett.105.136805.

[34] H. Peelaers, C.G. Van de Walle, Effects of strain on band structure and effective masses in MoS, Phys. Rev. B 86 (2012) 241401, https://doi.org/10.1103/PhysRevB.86.241401.

[35] S.F. Pugh, XCII. Relations between the elastic moduli and the plastic properties of polycrystalline pure metals, Lond. Edinb. Dublin Philos. Mag. J. Sci. 45 (1954) 823–843, https://doi.org/10.1080/14786440808520496.

[36] A. Bafekry, S. Farjami Shayesteh, F.M. Peeters, Electronic, optical and thermoelectric properties of layered BaI_2 compound, Chem. Phys. 526 (2019) 110442, https://doi.org/10.1016/j.chemphys.2019.110442.

[37] D.R. Clarke, Materials selection guidelines for low thermal conductivity thermal barrier coatings, Surf. Coat. Technol. 163–164 (2003) 67–74.

[38] D.G. Cahill, S.K. Watson, R.O. Pohl, Lower limit to the thermal conductivity of disordered crystals, Phys. Rev. B 46 (1992) 6131–6140.

[39] Aysenur Gencer, Ozge Surucu, Gokhan Surucu, Engin Deligoz, Anisotropic mechanical properties of Tl4Ag18Te11 compound with low thermal conductivity, J. Solid. State Chem. 289 (2020) 121469, https://doi.org/10.1016/j.jssc.2020.121469.

[40] B. Ghebouli, M.A. Ghebouli, T. Chihi, M. Fatmi, S. Boucetta, M. Reffas, First-principles study of structural, elastic, electronic and optical properties of SrMO3 (M=Ti and Sn), Solid. State Commun. 149 (47–48) (2009) 2244–2249, https://doi.org/10.1016/j.ssc.2009.09.001.

[41] H. Shi, H. Pan, Y.W. Zhang, B.I. Yakobson, Quasiparticle band structures and optical properties of strained monolayer MoS_2 and WS_2, Phys. Rev. B 87 (2013) 155304 https://doi.org/10.1103/PhysRevB.87.155304.

[42] H.B. Mabiala-Poaty, D.H. Douma, B. M'Passi-Mabiala, R.E. Mapasha, Structural and electronic properties of SnS_2 stacked nanosheets: an ab-initio study, J. Phys. Chem. Solids (2018).

[43] R. Fei, W. Li, J. Li, L. Yang, Giant piezoelectricity of monolayer group IV monochalcogenides: SnSe, SnS, GeSe, and GeS, Appl. Phys. Lett. 107 (2015) 173104, https://doi.org/10.1063/1.4934750.

[44] L.C. Gomes, A. Carvalho, A.H. Castro Neto, Enhanced piezoelectricity and modified dielectric screening of two-dimensional group-IV monochalcogenides, Phys. Rev. B 92 (2015) 214103, https://doi.org/10.1103/PhysRevB.92.214103.

[45] H. Ozisik, M. Caid, E. Deligoz, D. Rached, Y. Rached, Unveiling the Potential of Ba2Zn5As6 and Ba2Zn5Sb6: a comprehensive DFT Study, Adv. Theory Simul. 8 (2025) 2401099, https://doi.org/10.1002/adts.202401099.

[46] M. Bernardi, M. Palummo, J.C. Grossman, Extraordinary sunlight absorption and one nanometer thick photovoltaics using two-dimensional monolayer materials, Nano Lett. 13 (2013) 3664–3670, https://doi.org/10.1021/nl401544y.

[47] V. Tran, R. Soklaski, Y. Liang, L. Yang, Layer-controlled band gap and anisotropic excitons in few-layer black phosphorus, Phys. Rev. B 89 (2014) 235319, https://doi.org/10.1103/PhysRevB.89.235319.

[48] X. Li, S. Li, J. Chen, Z. Ma, D. Wang, P. Lu, W. Chen, B. Bian, First-principles study on photocatalytic performance of direct Z-scheme GaX/SnS_2 (X = N, P, As), Colloids Surf. A Physicochem. Eng. Asp. (2025).

[49] T. Deng, C. Qin, L. Sun, L.-X. Liu, W. Zhan, G. Zhuang, J. Jia, X. Han, Operando structural evolution of octahedral SnS_2/SnO_2 heterojunctions enabling efficient CO_2-to-formate conversion over a broad potential window, Nano Res. 19 (2026) 94907848, https://doi.org/10.26599/NR.2025.94907848.